

Ultrathin carbon foams for effective electromagnetic interference shielding

Yang Li ^a, Bin Shen ^{a,*}, Xueliang Pei ^b, Yonggang Zhang ^b, Da Yi ^c, Wentao Zhai ^{a, **}, Lihua Zhang ^a, Xingchang Wei ^c, Wenge Zheng ^{a, ***}

^a Ningbo Key Lab of Polymer Materials, Ningbo Institute of Material Technology and Engineering, Chinese Academy of Sciences, Ningbo 315201, China
^b National Engineering Laboratory of Carbon Fiber Preparation Technology, Ningbo Institute of Material Technology and Engineering, Chinese Academy of Sciences, Ningbo 315201, China

^c College of Information Science and Electronic Engineering, Zhejiang University, Hangzhou 310027, China

ABSTRACT

Ultrathin carbon foams with the thickness about 24 μm were fabricated by the pyrolysis of polyimide/graphene composite foams. The addition of graphene was verified to stabilize the porous structure of the foams and accelerate their graphitization process simultaneously. Consequently, the well-defined carbon foams exhibited much higher electromagnetic interference (EMI) shielding effectiveness (SE) up to 24 dB over the frequency range of 8–12 GHz, in comparison with the non-foamed counterparts. The possible mechanism behind the phenomenon was attributed to their enhanced microwave absorption via the internal multiple scattering and reflections. Moreover, the SE could be further improved to 43 and 51 dB by increasing the sample thickness gradually to 51 and 73 μm , respectively. The carbon foams with high thermal stability are very promising in the fabrication of ultrathin EMI shields for thermally harsh applications.

1. Introduction

The rapid increase of wireless communication devices (e.g. smartphones, laptop computers and wireless routers) has caused severe electromagnetic pollution to their surroundings, threatening information security and human beings' health. Therefore, electromagnetic interference (EMI) shielding materials are eagerly needed [1]. Metals are the most common EMI shields, but they always suffer from large density, poor resistance to corrosion and expensive cost to process. As alternatives, carbon materials, such as carbon black, carbon fibers (CFs), carbon nanofibers (CNFs), carbon nanotubes (CNTs) and graphene, have been explored and blended with polymers as conductive fillers for the purpose of fabricating lightweight and tough polymer-based shielding materials. Particularly, the fillers with high aspect ratio like CNTs and graphene are more preferred, due to the skin effect which refers to the

phenomenon that high-frequency EM waves tend to interact with the near surface region of a shield [2,3].

Recently, the EMI shielding materials with strong absorption have drawn considerable attention due to their weak secondary reflection [4]. In the fabrication of such materials, some researchers prefer to fabricate polymer-based shielding foams [5–9]. In foaming shields, conductive fillers are concentrated in the cell walls, which enhances the internal multiple scattering and reflections, and eventually their EMI shielding performance. Moreover, porous structure can also render these materials with low density, high flexibility and excellent impact resistance [10]. For example, the polypropylene (PP)/10 vol.% CF composite foam fabricated by Ameli et al. using foam injection molding absorbed approximately 81% incident EM energy, which was about 10% higher than that of the solid counterpart [11]. Owing to the enhanced absorption, the foam exhibited an effective shielding effectiveness (SE) of 25 dB over the frequency range of 8–12 GHz (the X band range), much higher than that of the solid (20 dB). Similar phenomenon was also observed in PP/stainless-steel fiber foams [12]. Additionally, Ling et al. fabricated microcellular polyetherimide (PEI)/graphene foams by phase separation and the results revealed that about 90.6–98.9% incident EM energy was absorbed by the foams, which was much higher

* Corresponding author.

** Corresponding author.

*** Corresponding author.

E-mail addresses: shenbin@nimte.ac.cn (B. Shen), wtzhai@nimte.ac.cn (W. Zhai), wgzheng@nimte.ac.cn (W. Zheng).

than the 76.2–90.8% for the solids in control [13].

Despite the great progress in polymer-based shielding materials, there are still some issues needing to be settled. Since a high electrical conductivity is necessary for high-performance EMI shielding materials, most current polymers are electrically insulating. Thereby, most polymer-based composites including solids and foams require both a high filler loading (≥ 10 wt.%) to form effective conductive networks and a large thickness (≥ 2 mm) to meet the commercial level of 20 dB [10–20]. Consequently, the excessive filler raises significant difficulties in processing, while the large thickness increases the volume of the shields, making them unavailable for the application of microelectronics. Moreover, the low thermal stability of polymers, as well as their weak flame retardation, also makes the resulting materials unable to work continuously, for some absorbed EM energy can be transformed into heat and lead to fire. With modern electronics getting smaller, thinner and faster, it has posed a challenge to fabricate lightweight and effective EMI shielding materials with low thickness, high thermal stability and strong microwave absorption.

Carbon-based materials, such as flexible graphite, CNT and graphene papers, have superior thermal and electrical properties. When utilized as EMI shields, these materials generally exhibit effective SE (≥ 20 dB) in extremely low sample thickness (0.02–0.79 mm) [21–24]. More importantly, the SE still remains excellent under thermally harsh conditions [25–27]. These unique properties make them good candidates in replacing polymer-based materials for EMI shielding application. After made into hydrogels and aerogels, carbon-based composites are fairly promising in energy storage, gas separation and catalyst beds [28–33]. More recently, porous carbon-based shields with ultralow density for EMI shielding have been reported. For example, with a template method, Chen et al. prepared poly(dimethyl siloxane) (PDMS) coating graphene foams in which the graphene skeleton was made by chemical vapor deposition (CVD) [34]. The as-prepared foam with low density of 0.06 g cm^{-3} exhibited a SE of 20 dB in a low thickness of 1 mm. Due to the synergetic effect of electrical conductivity and multiple reflections, most carbon-based shielding foams possessed an absorption-predominant shielding mechanism [34–36]. These results convince us that carbon foams may be a good option to fulfill our target of fabricating lightweight EMI shields with low thickness, effective SE and strong microwave absorption for thermally harsh applications. Moreover, the porous structure may also render themselves with other functions like energy storage [37].

Aromatic polyimides (PIs) are commonly employed as carbon precursors to prepare carbon foams, due to their high carbon yield (to guarantee sufficient residues), solid-state carbonization (to keep the shape of the precursor) and better-defined molecular structure than pitches (to obtain more simple carbonization behavior and high quality carbon products) [38,39]. One commercially available aromatic PI film “Kapton” is very prevailing in the manufacture of high quality graphite films, due to its flat molecule structure, high degree of molecular orientation and simple release of noncarbon atoms during carbonization and graphitization [40–42]. As the film is synthesized by anhydride and diamine, thus pyromellitic dianhydride (PMDA) and 4,4'-oxydiamine (ODA), it is also called PMDA/ODA type PI. To date, several kinds of carbon foams have already been obtained from PMDA/ODA type PI by thermal decomposition, but the heat treatment temperatures (HTTs) during the process are relatively low (≤ 1000 °C) and their applications are frequently limited to gas absorption and catalytic supports [38,43–46]. Therefore, it is interesting to study the carbonization and graphitization behaviors of the foams at much higher HTTs and investigate their EMI shielding performance simultaneously.

In our previous work [47], microcellular PMDA/ODA type PI/

graphene composite foams (PIGFs) were fabricated by the combination of *in situ* polymerization and phase separation. Based on this, we prepared carbon foams in this work by thermally decomposing the PIGFs at various temperatures ranging from 1000 to 2600 °C. Graphene was used to stabilize the porous structure of the foams and accelerate their graphitization process, for we found that graphene could effectively suppress the shrinkage of PI film during its pyrolysis and even possibly accelerate its graphitization process [48]. As a result, the as-obtained ultrathin carbon foams with well-defined porous structure exhibited effective SE and excellent thermal stability. By comparing the SE of the foams with that of the solid counterparts, we found that porous structure is greatly necessary for fabricating EMI shielding materials with strong microwave absorption.

2. Experimental

2.1. Materials

Graphite oxide was synthesized via a modified Hummers method [49]. PMDA, ODA and N,N'-dimethylformamide (DMF) were purchased from Sinopharm Chemical Reagent (China). All chemicals were used as received without further purification.

2.2. Fabrication of PI/graphene composite precursors

The preparation of PIGFs was similar to our previous report [47]. In the typical procedure (Fig. 1), graphite oxide was dispersed in DMF and fully exfoliated into graphene oxide (GO) with the help of ultrasonication for 30 min. ODA and PMDA monomers in equal mole ratio were added subsequently to synthesize poly(amic acid) (PAA), the precursor of PI. The solid content was about 10%. The synthesized PAA/GO casting solution was then cast on a glass substrate and immediately impregnated into a coagulant bath composed of alcohol and distilled water (with a volume ratio of 1:1) for 20 min, in order to obtain microcellular PAA/GO foam. The PAA/GO foam was then dried at 60 °C and further thermally imidized at 350 °C for 30 min, during which PAA was transformed into PI and GO was reduced to graphene. Consequently, PIGFs with graphene loading of 0, 1, 2 and 4 wt.% were prepared and termed as PIGF0, PIGF1, PIGF2 and PIGF4, respectively. The thickness for the PIGFs was about 45 μm .

As control, PI/graphene solids (PIGSs) were also prepared by the direct thermal imidization of PAA/GO casting solutions on glass substrate. As a result, PIGSs including PIGS0, PIGS1, PIGS2 and PIGS4 were prepared and their thickness was about 12 μm . Here need to mention that the PIGFs had an identical compressed thickness with that of PIGSs. All the samples were used as precursors and ready for carbonization and graphitization.

2.3. Carbonization and graphitization of PI/graphene composites

In this process, PIGFs and PIGSs were sandwiched among artificial polished graphite plates and pyrolyzed at the temperatures of 1000, 1500, 2100 and 2600 °C, respectively, in flowing high purity nitrogen. For each temperature, the samples were cured for 1 h.

3. Characterization

3.1. Scanning electron microscopy

The scanning electron microscopy (SEM) observation was performed with a Hitachi S-4800 field emission SEM at an accelerating voltage of 8 kV. Prior to the observation, all samples needed to be freeze-fractured with liquid nitrogen to obtain flat cross-section.

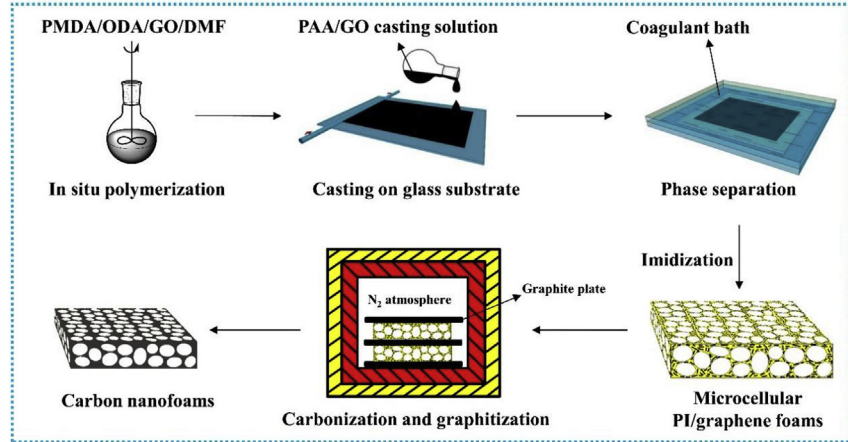


Fig. 1. Sketch for the preparation of carbon foams from PIGFs via the combination of *in situ* polymerization, phase separation, thermal imidization and decomposition. (A colour version of this figure can be viewed online).

The as-obtained samples were then dried at 100 °C for 2 h to remove residual water as much as possible and coated with platinum. The cell density (N_0), thus the number of cells per cubic centimeter, was determined from SEM micrographs and calculated using the equation as follows [50]:

$$N_0 = [nM^2/A]^{3/2} \times \phi \quad (1)$$

where n is the number of cells in the SEM image, M is the magnification factor, A is the area of micrograph (cm^2), and ϕ is the expansion ratio and can be expressed as:

$$\phi = \rho/\rho_f \quad (2)$$

where ρ is the density of solid materials and ρ_f is the density of foaming materials. In this study, the density was calculated geometrically.

3.2. X-ray diffraction

The X-ray diffraction (XRD) measurement was conducted using a Bruker AXS X-ray diffractometer with $\text{Cu K}\alpha$ radiation ($\lambda = 0.154178 \text{ nm}$) at the generator voltage of 40 kV and the current of 40 mA. The diffraction patterns of all samples were recorded at room temperature in the 2θ ranging from 10 to 80°. The curves needed to be calibrated with silicone powder before use. The interlayer spacing of (002) plane d_{002} was calculated by Bragg's law [51]:

$$d = \lambda/2\sin\theta \quad (3)$$

where λ is 0.154178 nm. The through-plane crystalline size L_c , the stacking thickness of graphene layer along the c -axis, was estimated with β_{002} (the half width of the (002) reflection) via the Debye–Scherrer formula [52]:

$$L_c = 0.89\lambda/\beta\cos\theta \quad (4)$$

3.3. Raman spectra

The Raman spectra were excited with a laser of 532 nm and recorded with Labram spectrometer in the range of

1000–3200 cm^{-1} . The in-plane crystalline size L_a , the graphitic coherent domains perpendicular to the c -axis, was calculated from the ratio of Raman intensities (integrated areas) I_D/I_G with the coefficient $C(\lambda)$ of 4.4 nm [52].

$$L_a = C(\lambda)/(I_D/I_G) \quad (5)$$

3.4. Electrical conductivity

The electrical conductivity of polymers composites was examined by an EST121 ultrahigh resistance and microcurrent meter (Beijing EST Science & Technology CO. Ltd.) according to ASTMD257, while that of carbonized and graphitized samples was recorded using a standard four-probe method on a Napson Cresbox Measurement System.

3.5. EMI shielding performance

The EMI SE was measured with a R&S ZVA67 vector network analyzer (VNA) in the X band using the wave guide. All samples were cut into rectangle plates with a dimension of 22.5 mm × 10.0 mm to fit the sample holder. The thickness of the PIGFs heat-treated at 2600 °C gained from the SEM images was about 24 μm , while that for the graphitized PIGFs was 7 μm . All these values were obtained from the measurement of their SEM images.

The EMI SE (SE_T) refers to the logarithm of the ratio of incoming power (P_i) to transmitted power (P_t) of radiation, which is the sum of the absorption (SE_A), the reflection (SE_R) and the multiple reflections (SE_M) [19]:

$$\text{SE}_T = 10 \log(P_i/P_t) = \text{SE}_A + \text{SE}_R + \text{SE}_M \quad (6)$$

The power coefficients of reflectivity (R), transmissivity (T), and absorptivity (A) are determined using S parameters (S_{11} , S_{22} , S_{12} and S_{21}) with the equations as follows [53]:

$$R = |S_{11}|^2 = |S_{22}|^2 \quad (7)$$

$$T = |S_{12}|^2 = |S_{21}|^2 \quad (8)$$

$$R + T + A = 1 \quad (9)$$

In the case of $SE_T \geq 15$ dB, SE_M is usually neglected and SE_T can be simplified as:

$$SE_T \approx SE_A + SE_R \quad (10)$$

The corresponding effective absorptivity (A_{eff}), SE_R and SE_A can be written as:

$$A_{\text{eff}} = (1 - R - T)/(1 - R) \quad (11)$$

$$SE_R = -10\log(1 - R) \quad (12)$$

$$SE_A = -10\log(1 - A_{\text{eff}}) = -10\log[T/(1 - R)] \quad (13)$$

Additionally, the skin depth (δ) of a shield, defined as the depth at which electromagnetic energy drops exponentially to $1/e$ of its incident value, was roughly evaluated according to the following relation [2]:

$$\delta = (\pi\sigma f\mu)^{-1/2} \quad (14)$$

where σ is the electrical conductivity, f is the frequency and μ is the magnetic permeability.

3.6. Thermal stability

The thermal stability of the PIGFs heat-treated at 2600 °C was measured with a Mettler-Toledo TG/DSC1 analyzer (Switzerland) from 100 to 1000 °C at a heating rate of 20 °C min⁻¹ under an oxidative (air) atmosphere.

4. Results and discuss

4.1. Carbonization and graphitization behaviors of PIGFs

Previous reports reveal that an abrupt weight decrease will happen to Kapton type PI film during its pyrolysis process, due to the release of decomposition gases like CO, CO₂, and N₂ [39,54]. Furthermore, this process is always accompanied by pronounced shrinkage along the film. For example, about 15–18% liner shrinkage has been reported for the aromatic PI films carbonized at 1000 °C, which corresponds to the 39–45% volumetric shrinkage [55]. The large shrinkage could possibly cause the collapse of the porous structure of PI foam during its pyrolysis process. Therefore, graphene was introduced to stabilize the porous structure. To verify its feasibility, PIGF4 was initially selected as a representative sample and its structure evolution at varying HTTs was investigated.

As shown in Fig. 2, the porous structure of PIGF4 is well preserved, even when the HTT is up to 2600 °C. Moreover, the whole process can be divided into three stages in terms of HTTs: 350 °C, 1000–1500 °C, and 2100–2600 °C. The HTT of 350 °C corresponds to primary PIGF4, which shows an average cell size of 1.8 μm and a cell density of 3.3×10^{11} cells cm⁻³. After the carbonization in the HTT range of 1000–1500 °C, these values marginally become to ca. 1.5 μm and 5.0×10^{11} cells cm⁻³, indicating a slight shrinkage in the foam. This is quite different from the large shrinkage in pristine PI film [39], possibly due to the rigid structure of graphene that has significantly restrained the shrinkage of PIGF4. Furthermore, the smooth fracture in the magnified SEM images also suggests the brittle feature of the carbonized samples.

When the HTT further increases to 2100–2600 °C, pronounced shrinkage is observed, as supported by the distinct changes in the values of cell size (ca. 0.6 μm) and cell density (ca. 1.0×10^{13} cells cm⁻³). According to previous report [56], a thinning process is often observed in the thickness of Kapton film during its graphitization

process. Therefore, the large shrinkage may be assigned to the occurrence of graphitization of PIGF4. Moreover, a sharp brittle-tough transition is also observed in their SEM images with higher magnification, further confirming the development of graphitic structure [57]. In the whole process, the density increases gradually from 0.40 g cm⁻³ for primary PIGF4 to 0.61 g cm⁻³ for the carbonized samples, and consequently to 0.72 g cm⁻³ for the graphitized ones.

In Fig. 3a, XRD patterns were employed to make more detailed investigation. For primary PIGF4, there are three typical peaks at $2\theta = 14.74^\circ$, 22.44° and 26.48° , suggesting the high degree of the orientation of PI molecules, which lays a good foundation for the following carbonization and graphitization of PIGF4 [58–60]. After the carbonization at 1000 °C, PIGF4 is converted into amorphous carbon, as proved by the two broad peaks at around $2\theta = 25.7^\circ$ (002) and 43.6° (100). When the HTT further increases to 1500 °C, the arrangement of the basic structural units (BSUs) in carbonized PIGF4 is considerably improved. Furthermore, the unsymmetrical (002) peak is related to the varying degree of the orientation of BSUs [61]. After the graphitization above 2000 °C, the main peak (002) becomes much sharper and shifts to higher angles, indicating the higher degree of the orientation of BSUs. Specifically, the interlayer spacing d_{002} for the PIGF4 graphitized at 2100 °C reaches to 0.3385 nm. This value is comparable to the value of graphite crystal (0.3386 nm) achieved by Konno et al. from PMDA/ODA type PI at 2500 °C [62], probably owing to the catalytic effect of graphene on the graphitization process of PI. With the HTT up to 2600 °C, the d_{002} decreases to 0.3370 nm, very approaching to that of ideal graphite (0.3354 nm).

In Fig. 3b, Raman spectra were recorded to investigate the graphitization degree of PIGF4. Apparently, each Raman spectrum involves the G-band (associated with the stretching of sp²-hybridized carbon atoms in graphitic 2D hexagonal lattice) at 1580–1595 cm⁻¹ and the D-band (associated with the sheering of sp³-hybridized carbon atoms in amorphous carbon and defects) at 1320–1330 cm⁻¹ alike [63]. The intensity ratio of the D-band to G-band (I_D/I_G), inverse to the average size of crystalline carbon, was calculated after peak separation. As seen, the I_D/I_G increases with the increase in HTT. Moreover, the G-band shifts gradually from 1594 cm⁻¹ for the sample treated at 1000 °C to 1580 cm⁻¹ for that at 2600 °C. All the results demonstrate the increased ordered domains of carbon layers in the pyrolyzed sample. Besides, in the second-order Raman spectra, the intensity of the symmetric G-band at around 2660 cm⁻¹ increases progressively at elevated HTTs. As we know, the nature graphite with AB stacking possesses a highly asymmetric G-band that can be fitted into two Lorentz peaks [1]. The G-band in our graphitized samples (Fig. 3b), however, is only one single peak, indicating the coexistence of crystalline and turbostratic structures.

Generally speaking, the pyrolysis of our PIGFs is composed of the carbonization and graphitization process. The carbonization process can further be divided into two portions: the pyrolysis of PI molecules and carbonization. The former usually occurs over the HTT range of 500–700 °C and is due to the breakage of the carbonyl groups in the imide part and the ether oxygen in the bridging part, while the latter results mainly from the decomposition of the imide groups in PI molecule at the temperature over 700 °C [39,64]. This process is usually accompanied by an abrupt decrease in weight, a sudden increase in density and an evolution of a large amount of decomposition gases. Moreover, the stacking of the carbon layers is turbostratic, even after the carbonization at 1500 °C. It is not until the HTT above 2000 °C that turbostratic carbon begins to transform into crystalline graphite, giving rise to the partially graphitization of PIGFs. According to the graphitization mechanism of Kapton film proposed by Bourgerette et al. [56], tiny pores are often formed in

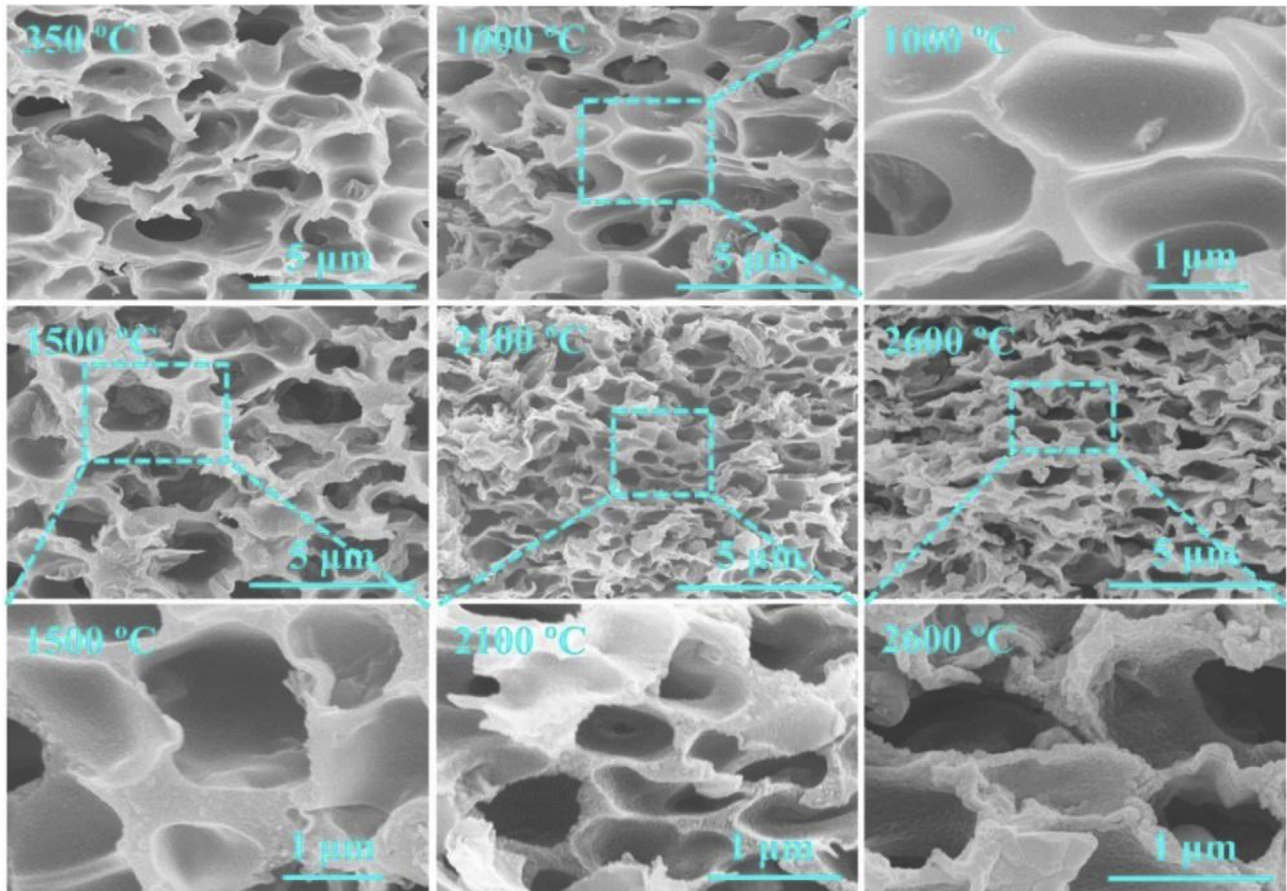


Fig. 2. SEM micrographs of the porous structure of the PIGF4 pyrolyzed at various HTTs ranging from 1000 to 2600 °C. As a control, primary PIGF4 was also presented as the HTT of 350 °C. (A color version of this figure can be viewed online).

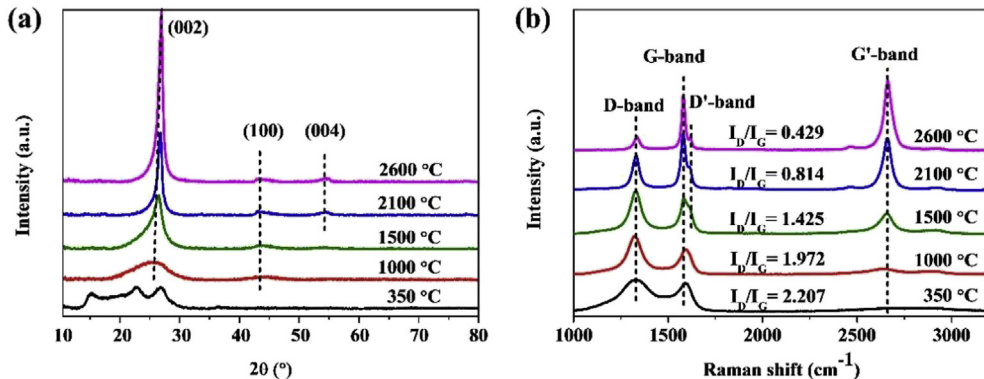


Fig. 3. XRD patterns (a) and Raman spectra (b) of the PIGF4 treated at different HTTs. Among these, the HTT of 350 °C corresponds to primary PIGF4. (A colour version of this figure can be viewed online).

the stacks of turbostratic carbon layers that are flattened along the film surface with HTT approaching to the graphitization temperature. Once the pores collapsing, the turbostratic structure is suddenly transformed into graphitic, initializing the graphitization process. If the HTT further increases, the graphitic structure will be continuously developed until the arrival of the perfect graphitization.

4.2. Influence of graphene on the carbonization and graphitization process of PIGFs

To further confirm the assumption that graphene has stabilized

the porous structure of PIGFs during their pyrolysis, the SEM images of the samples heat-treated at 350, 1500 and 2600 °C, have been shown in Fig. 4. For PIGF precursors, the cell density in Fig. 4a–d tends to increase with graphene content increasing, fairly similar to our previous work [47]. Particularly, the samples with more graphene sheets display rough cell walls (dotted circles in Fig. 4c and d). When carbonized at 1500 °C, the foams exhibit smaller cell size and higher cell density (Fig. 4e–h). For example, the average cell size of the carbonized PIGF0 decreases from 1.9 to 1.4 μm, about 26% decrease, while the corresponding cell density increases from 1.7×10^{11} to 5.1×10^{11} cells cm^{-3} , about 200% increase. In the case of carbonized PIGF1, these changes dramatically

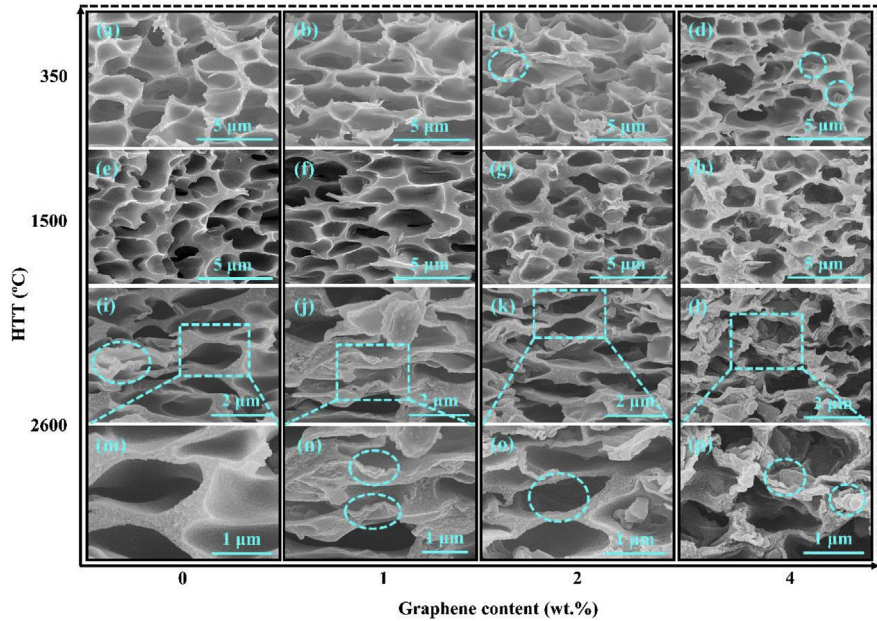


Fig. 4. SEM images of the PIGFs treated at different HTTs: 350 °C (a–d), 1500 °C (e–h) and 2600 °C (i–l), respectively. To make clear observation, magnified images (m–p) were also given to the samples graphitized at 2600 °C. (A colour version of this figure can be viewed online).

decrease to 11% for the cell size and 60% for the cell density. Further increasing graphene content may lead to much smaller change in both parameters. These phenomena demonstrate that the rigid structure of graphene does certainly have suppressed the shrinkage of PI foam during the carbonization process.

After the graphitization at 2600 °C, the cell size decreases to about 0.6 μm and the cell density increases to 1.0×10^{13} cells cm⁻³. Some cell deformation (the dotted circles in Fig. 4i) is observed in graphitized PIGF0, because of the more compact stacking of carbon layers. By comparing Fig. 4i–l, it is found that the graphitized samples with higher graphene content have a better-defined porous structure, fulfilling our original design of using graphene to stabilize the porous structure of carbon foams. In addition, ductile fracture, as well as layer-like structure, is observed in Fig. 4n–p, instead of in Fig. 4m. It is possibly due to the catalytic effect of graphene on the graphitization of PI, but more evidences are needed for this hypothesis.

Fig. 5 gives the XRD patterns and Raman spectra of the PIGFs treated at 1500 and 2600 °C, respectively. As shown in Fig. 5a, the PIGFs carbonized 1500 °C generally exhibit sharper (002) diffraction after the incorporation of graphene. Meanwhile, the peak position shifts gradually to higher angles as well. Furthermore, the corresponding I_D/I_G ratio in Raman spectra (Fig. 5b) shows a decreasing tendency with increasing graphene content, and the G-band red shifts gradually from 1599.4 to 1593.1 cm⁻¹. Similar phenomena are also observed in the subsequent graphitization process, as shown in Fig. 5c and d. To quantitatively analyze the changes in graphitized PIGFs, Table 1 lists their structure parameters. It is evident that the interlayer spacing d_{002} , through-plane crystallite size L_c , in-plane crystallite size L_a and the full width at half maximum (FWHM) of G-band are largely dependent on the content of graphene. Generally, the more the graphene in PI precursor, the higher the graphitization degree of the resultant graphitized samples. All the results demonstrate that graphene has a catalytic effect on the graphitization process of PI.

It has been said that the internal stress in the composite materials made of carbon fillers and carbon precursors can promote their graphitization process [65,66]. Actually, most of the internal

stress exists in the interfaces between the filler and precursors, which can be substantially accumulated during carbonization. Therefore, their graphitization frequently starts from the interfaces [65]. In this study, the biaxial stretching may be developed from PI matrix to graphene filler in the fabrication of PIGFs [47]. Furthermore, the rigid structure of graphene, as well as its large surface area, can effectively suppress the shrinkage of PI during thermal imidization and carbonization process [47,48], which causes the significant accumulation of internal stress on the interfaces between PI and graphene. Consequently, the graphitization process of our PIGFs was accelerated by graphene.

4.3. Electrical conductivity

The electrical conductivity of shielding materials has an intimate connection with their EMI shielding performance [2,3]. Thereby, the electrical conductivity of the PIGFs treated at different HTTs was tested before the measurement of the EMI SE. Since PI is an excellent electrical insulator, PIGF0 shows an extremely low electrical conductivity of 3.2×10^{-18} S cm⁻¹ (Fig. 6a). After the addition of graphene, several orders of magnitude are observed in their conductivity, owing to the construction of conductive network in PI matrix. Once the foams are carbonized at 1000 °C, their conductivity will be noticeably increased by more than five orders of magnitude. This increment is a direct reflection of the structure change in PI chains, for the pyrolysis of PI molecules and its carbonization usually occur during this process [67]. With the HTT further increasing to 2600 °C, a relatively slight increase, about one order of magnitude, can be observed in the conductivity. The reason is due to their more compact stacking of carbon layers at elevated HTTs, which may reduce the electrical interface resistance among adjacent carbon layers and cause the conductivity increment.

Fig. 6b compares the in-plane electrical conductivity of graphitized PIGFs and PIGSs. The conductivity for graphitized PIGF0 is 140 S cm⁻¹, while that for graphitized PIGS1 dramatically increases to 1500 S cm⁻¹, more than one order of magnitude. With graphene content further increasing, less increase is still observed until the

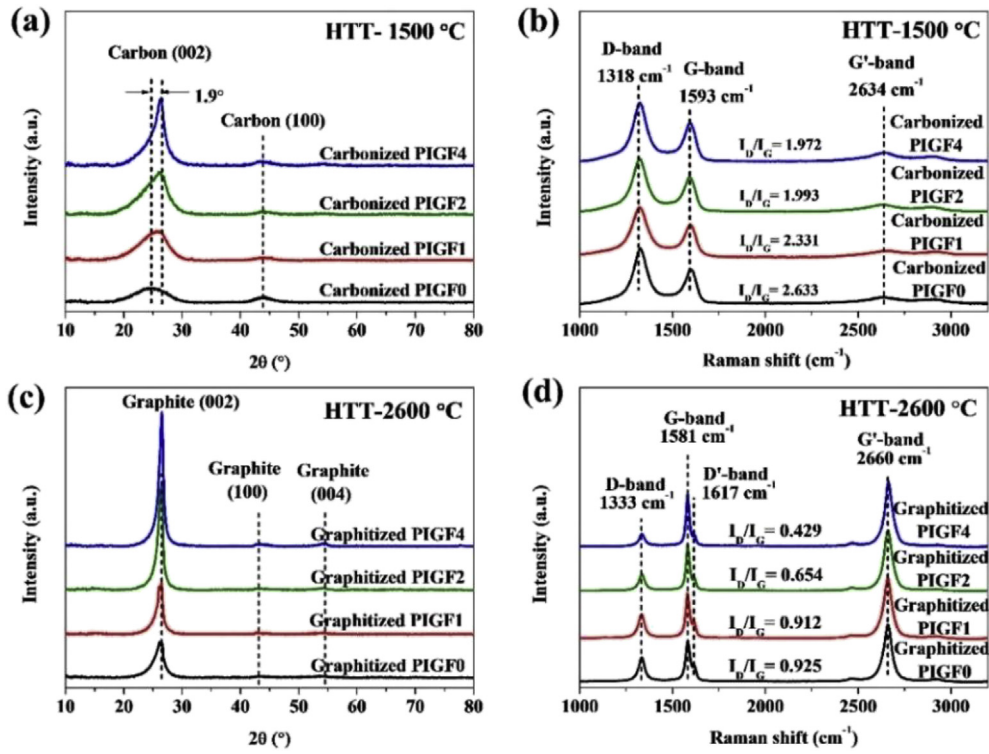


Fig. 5. XRD patterns (a, c) and Raman spectra (b, d) of PIGFs pyrolyzed at 1500 and 2600 °C, respectively. (A colour version of this figure can be viewed online).

Table 1

Structure parameters obtained from the XRD patterns and Raman spectra of the PIGFs graphitized at 2600 °C.

Precursors	XRD patterns			Raman spectra			
	2θ (°)	d_{002} (nm)	L_c (nm)	D-band (cm^{-1})	G-band (cm^{-1})	FWHM of G-band (cm^{-1})	L_a (nm)
PIGF0	26.10	0.3415	9.39	1334.6	1581.1	15.0	4.76
PIGF1	26.33	0.3385	9.92	1333.8	1581.0	13.1	4.82
PIGF2	26.38	0.3378	10.68	1333.5	1580.7	11.7	6.73
PIGF4	26.44	0.3370	11.84	1333.4	1580.0	11.1	10.26

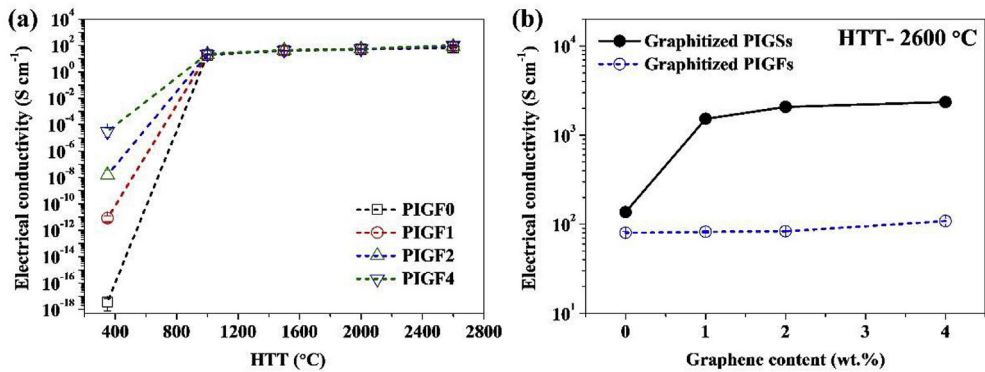


Fig. 6. In-plane electrical conductivity of the PIGFs treated at different HTTs (a) and that of the PIGFs and PIGSs graphitized at 2600 °C (b). (A colour version of this figure can be viewed online).

conductivity reaches to 2300 S cm^{-1} . The reason may be ascribed to the catalytic effect of graphene on the graphitization process of PI. In contrast, the electrical properties of graphitized PIGFs are quite different. For example, the conductivity for graphitized PIGFs is about 100 S cm^{-1} , and the addition of graphene just exerts marginal

impact on the conductivity. Additionally, the conductivity values of the foams are lower than those of the solids, which can be ascribed to their porous structure that may partially inhibit the ordered stacking of the carbon layers in the direction parallel to the surface of the foams and cause the increase in their contact resistance.

4.4. EMI shielding performance

To obtain sufficient EMI SE, we chose PIGF4 as an optimum carbon precursor and the shielding performance of the resultant carbon foams obtained at various HTTs was measured using the VNA in Fig. 7a. As shown in Fig. 7b, the foams generally exhibit much higher SE at elevated HTTs. Furthermore, the corresponding SE_A and SE_R at 9.0 GHz are given in Fig. 7c, where a great transition from reflection- to absorption-dominant shielding mechanism is observed with the increase in HTT. The main reason is due to their increased electrical conductivity at higher HTTs. As the conductivity is inversely proportional to the square of skin depth, a slight increase in the conductivity may result in a large decrease in the skin depth of a shield, and eventually an enhancement in its absorption contribution SE_A [68]. For example, the skin depth for the foam carbonized at 1000 °C is approximately 26 μm at 8.0 GHz, while for the sample at 2600 °C, this value decreases obviously to about 15 μm. The skin depth decrement has significantly enhanced their SE_A that is proportional to the skin depth [68]. Consequently, the foam exhibits a SE as high as 24 dB in the low thickness of 24 μm, as well as the absorption-dominant shielding mechanism.

In Fig. 7d, the SE of the PIGFs graphitized at 2600 °C is presented, in order to investigate the influence of graphene on the SE of the foams. As seen, the SE of graphitized PIGFs is highly dependent on the embedded graphene content. For instance, the average SE of graphitized PIGF0 is about 13 dB in the X band region. In the case of graphitized PIGF1, this value marginally increases to 15 dB. If more graphene is added, the SE can be dramatically improved to 20 dB for graphitized PIGF2 and 24 dB for graphitized PIGF4, respectively. Further investigation reveals that the effective absorptivity A_{eff} at 9.0 GHz is 0.84 for graphitized PIGF0, indicating that about 84% incident electromagnetic energy has been absorbed by the sample. For graphitized PIGF1, this value is 0.88. And much higher graphene content will cause a sudden increase in the A_{eff} , thus 0.96 for graphitized PIGF2 and 0.98 for graphitized PIGF4. These results demonstrate that the difference in the SE of graphitized PIGFs results mainly from the absorption contribution. Since the electrical conductivity of graphitized PIGFs is almost in the same level, the higher SE is possibly attributed to the better-defined porous structure at higher graphene content (Fig. 4k and l), which is able to significantly enhance their microwave absorption via the internal multiple reflections and scattering [2,10,11].

To further confirm the above assumption, the SE values of the non-foamed counterparts, the PIGSs graphitized at 2600 °C, were also researched. The result in Fig. 7e shows that, with the graphene content increasing, the SE of graphitized PIGSs also exhibits an increasing tendency ranging from around 12 dB for graphitized PIGS0 to 18 dB for graphitized PIGS4. As the tendency is similar to that in their conductivity (Fig. 6b), the increase in the SE is ascribed to their increased electrical conductivity at higher graphene content. More importantly, by comparing the SE of graphitized PIGSs and PIGFs, it is found that the SE is higher for graphitized PIGFs, even though graphitized PIGSs possess higher electrical conductivity. To gain insight into this phenomenon, their SE_A and SE_R at 9.0 GHz are analyzed in Fig. 7f, where both the SE_A and SE_R increase with the increase in graphene content. Moreover, the SE_A accounts for much higher proportion than the SE_R does, not only for graphitized PIGFs, but also for graphitized PIGSs. For example, about 84–98% incident electromagnetic energy has been absorbed by the foams, while this value for the solid counterparts is solely 80–87%. This result certainly affirms that the major difference among the SE of our carbon shields is the microwave absorption SE_A that is closely related to their inherent characteristics.

According to EMI shielding mechanisms, the SE_A stems mainly from dielectric loss and magnetic loss [4]. Due to the nonmagnetic

characteristic of our carbon shields, their SE_A highly depends on the dielectric loss that involves relaxation and conduction loss, influenced by polarization and conductivity, respectively. Furthermore, the polarization derives from defects, interfaces and functional groups [25,26]. The high conductivity of our carbon materials contributes a lot to the conduction loss, while the residual defects in the carbon layers after graphitization, as well as the interfaces between graphene and carbon matrix, can also induce the polarization to some extent and contribute to the relaxation loss. Additionally, the structure of a shield also has a great impact on the dielectric loss [10,20]. For EMI shielding foams, porous structure can significantly enhance the internal multiple scattering and reflections that are frequently ignored in the case of solid shields [8,69], resulting in the higher SE_A and SE_T (Fig. 7f). Furthermore, some researchers believe that the porous structure can effectively reduce the impedance mismatch of shielding materials and the ambient atmosphere, leading to the enhancement in their microwave absorption [7,70].

Table 2 makes a comparison of the SE of various solids and foams in the X band, from which we can see clearly that carbon-based materials generally exhibited far more advantages than polymer-based ones do, in fabricating ultrathin EMI shields. In the present work, an effective SE of 24 dB was obtained by our carbon foam with the sample thickness only of 24 μm in the X band region. Moreover, multilayered carbon composites have also been fabricated by bonding two or three layers of the PIGF4 graphitized at 2600 °C together using polyurethane (PU) gel. Consequently, the SE values of our carbon foams can be dramatically improved from 24 to 51 dB by increasing the thickness of graphitized PIGF4 gradually from 24 to 73 μm (Fig. 7g). Although both SE_A and SE_T contribute a lot to the SE_T , the SE_T increment is turned out to be dominated by the SE_A as shown in Fig. 7h. Considering the proportional relationship between the SE_A and SE_T [35], there is no doubt that the SE_A contributes more to the SE_T increment than the SE_R does for our multilayered carbon foams. In short, the sample thickness of the above carbon foams is generally in tens of micrometers, which is about two orders magnitude lower than that of polymer-based shields, making it the thinnest EMI shielding foam that has ever been reported to the best of our knowledge.

4.5. Thermal stability

In practical applications, high thermal stability is generally necessary for high-performance EMI shielding materials. So the thermostability of our graphitized PIGFs was also investigated using thermogravimetric analyzer (TGA) under an oxidative (air) atmosphere. As shown in Fig. 8, all the foams are thermally stable when the temperature is up to 550 °C. Moreover, the samples with graphene generally possess higher decomposition temperature. For example, the 5% weight loss temperature for graphitized PIGF0 is 661 °C, while this value is dramatically improved to 700 °C for graphitized PIGF1, 726 °C for graphitized PIGF2, and eventually, 754 °C for graphitized PIGF4. Similar phenomenon has also been declared by Kumar et al. in the carbon foams decorated with CNT and ferrocene, respectively, and the interior graphitic structure is believed to be responsible for the high thermal stability of the foams [73,74]. Generally, the higher the graphitization degree, the higher the thermal stability. This may be the possible reason why some of our carbon foams, whose graphitization has been accelerated by graphene, show much higher thermal stability than that without graphene does.

5. Conclusion

In summary, we have fabricated ultrathin carbon foams from

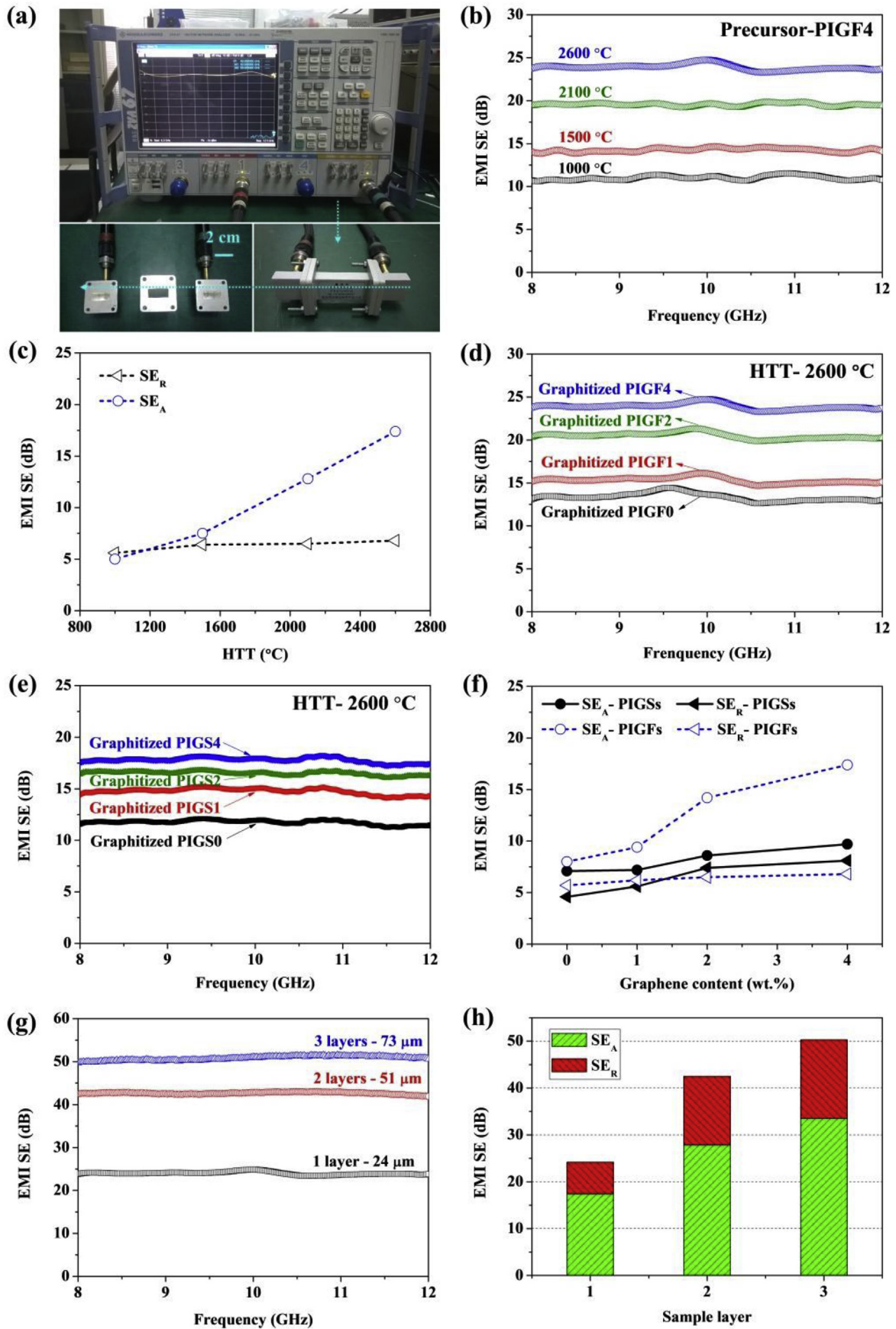


Fig. 7. Photograph of experimental setup (a); EMI SE of the PIGF4 treated at different HTTs in the X band (b); SE_A and SE_R of the PIGF4 treated at different HTTs at 9.0 GHz (c); EMI SE of the PIGFs (d) and PIGSs (e) graphitized at 2600 °C in the X band; SE_A and SE_R of the PIGSs and PIGFs graphitized at 2600 °C at 9.0 GHz (f); EMI SE of multilayered graphitized PIGF4 in different thicknesses: 24, 51 and 73 µm (g); SE_A and SE_R of multilayered graphitized PIGF4 at 9.0 GHz (h). (A colour version of this figure can be viewed online).

Table 2

EMI SE of various shielding materials in the forms of solids and foams in the X band region (PE: polyethylene, PS: polystyrene, PMMA: polymethylmethacrylate, PVDF: polyvinylidene fluoride).

EMI shields: Matrix/filler	Filler loading	Thickness (mm)	EMI SE (dB)	References
Solid	Epoxy/graphene	15 wt.%	/	[15]
	PMMA/graphene	4.23 vol.%	3.4	[71]
	PU/graphene	5.0 vol.%	2.0	[72]
	PE/CNT	50 wt.%	0.025	[22]
	Graphene	/	0.008	[1]
	Carbon/graphene	/	0.007	This study
Foam	PS/CNF	15 wt.%	/	[6]
	PS/CNT	7 wt.%	/	[5]
	PP/carbon fiber	10 vol.%	3.1	[11]
	PP/stainless-steel fiber	1.5 vol.%	3.1	[12]
	PS/graphene	30 wt.%	2.5	[17]
	PMMA/graphene	1.8 vol.%	2.5	[10]
	PVDF/graphene	7 wt.%	/	[9]
	PEI/graphene	10 wt.%	2.3	[13]
	PEI/graphene@Fe ₃ O ₄	10 wt.%	2.5	[8]
	PI/graphene	16 wt.%	0.8	[47]
	PDMS/graphene	0.8 wt.%	1.0	[34]
	Carbon	/	10	[36]
	Carbon/ferrocene	10 wt.%	2.75	[73]
	Carbon/CNT	0.5 wt.%	2.75	[74]
	Carbon/graphene	42 wt.%	3.0	[35]
	Carbon/graphene	/	0.024	This study
	Carbon/graphene	/	0.051	This study
	Carbon/graphene	/	0.073	This study

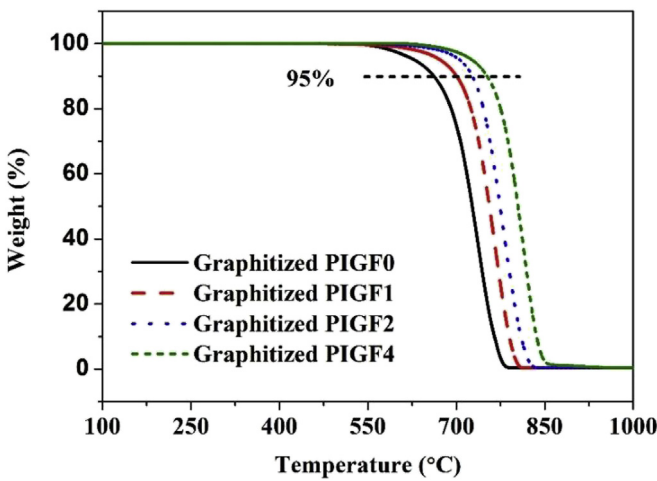


Fig. 8. TGA curves of the PIGFs graphitized at 2600 °C under oxidative (air) atmosphere. (A colour version of this figure can be viewed online).

PIGFs via thermal decomposition and investigated their EMI shielding performance. The results revealed that graphene could simultaneously help to stabilize the porous structure of the foams and facilitate their graphitization process via the internal stress between the matrix and fillers. As a consequence, the resultant carbon foam with well-defined porous structure and high thermal stability exhibited an effective SE of 24 dB in an ultralow thickness of 24 μm. Additionally, by comparing the SE of the foams with that of the solid counterparts, it was found that the foams possess much higher SE than the solid counterparts did. The reason was mainly due to the enhanced microwave absorption derived from the porous structure via multiple scattering and reflections. This work provides fairly useful information to the fabrication of ultrathin EMI shielding materials for thermally harsh environment.

Acknowledgments

Financial supports from the National Natural Science

Foundation of China (Grant No. 51473181, 51573202 and 61274110), National High Technology Research and Development Program of China (863 Program, Grant No. 2013AA032003), China Postdoctoral Science Foundation (Grant No. 2015M570531) are gratefully acknowledged.

References

- B. Shen, W.T. Zhai, W.G. Zheng, Ultrathin flexible graphene film: an excellent thermal conducting material with efficient EMI shielding, *Adv. Funct. Mater.* 24 (2014) 4542–4548.
- D.D.L. Chung, Electromagnetic interference shielding effectiveness of carbon materials, *Carbon* 39 (2001) 279–285.
- D.D.L. Chung, Carbon materials for structural self-sensing, electromagnetic shielding and thermal interfacing, *Carbon* 50 (2012) 3342–3353.
- M.S. Cao, X.X. Wang, W.Q. Cao, J. Yuan, Ultrathin graphene: electrical properties and highly efficient electromagnetic interference shielding, *J. Mater. Chem. C* 3 (2015) 6589–6599.
- Y.L. Yang, M.C. Gupta, K.L. Dudley, R.W. Lawrence, Novel carbon nanotube–polystyrene foam composites for electromagnetic interference shielding, *Nano Lett.* 5 (2005) 2131–2134.
- Y.L. Yang, M.C. Gupta, K.L. Dudley, R.W. Lawrence, Conductive carbon nanorib–polymer foam structures, *Adv. Mater.* 17 (2005) 1999–2003.
- J.M. Thomassin, C. Pagnoulle, L. Bednarz, I. Huynen, R. Jerome, C. Detrembleur, Foams of polycaprolactone/MWNT nanocomposites for efficient EMI reduction, *J. Mater. Chem.* 18 (2008) 792–796.
- B. Shen, W.T. Zhai, M.M. Tao, J.Q. Ling, W.G. Zheng, Lightweight, multifunctional polyetherimide/graphene@Fe₃O₄ composite foams for shielding of electromagnetic pollution, *ACS Appl. Mater. Interfaces* 5 (2013) 11383–11391.
- V. Eswaraiah, V. Sankaranarayanan, S. Ramaprabhu, Functionalized graphene–PVDF foam composites for EMI shielding, *Macromol. Mater. Eng.* 296 (2011) 894–898.
- H.B. Zhang, Q. Yan, W.G. Zheng, Z. He, Z.Z. Yu, Tough graphene–polymer microcellular foams for electromagnetic interference shielding, *ACS Appl. Mater. Interfaces* 3 (2011) 918–924.
- A. Ameli, P.U. Jung, C.B. Park, Electrical properties and electromagnetic interference shielding effectiveness of polypropylene/carbon fiber composite foams, *Carbon* 60 (2013) 379–391.
- A. Ameli, M. Nofar, S. Wang, C.B. Park, Lightweight polypropylene/stainless-steel fiber composite foams with low percolation for efficient electromagnetic interference shielding, *ACS Appl. Mater. Interfaces* 6 (2014) 11091–11100.
- J.Q. Ling, W.T. Zhai, W.W. Feng, B. Shen, J.F. Zhang, W.G. Zheng, Facile preparation of lightweight microcellular polyetherimide/graphene composite foams for electromagnetic interference shielding, *ACS Appl. Mater. Interfaces* 5 (2013) 2677–2684.
- N. Li, Y. Huang, F. Du, X.B. He, X. Lin, H.J. Gao, et al., Electromagnetic interference (EMI) shielding of single-walled carbon nanotube epoxy composites,

Nano Lett. 6 (2006) 1141–1145.

[15] J.J. Liang, Y. Wang, Y. Huang, Y.F. Ma, Z.F. Liu, F.M. Cai, et al., Electromagnetic interference shielding of graphene/epoxy composites, *Carbon* 47 (2009) 922–925.

[16] A.P. Singh, P. Garg, F. Alam, K. Singh, R.B. Mathur, R.P. Tandon, et al., Phenolic resin-based composite sheets filled with mixtures of reduced graphene oxide, gamma-Fe₂O₃ and carbon fibers for excellent electromagnetic interference shielding in the X-band, *Carbon* 50 (2012) 3868–3875.

[17] D.X. Yan, P.G. Ren, H. Pang, Q. Fu, M.B. Yang, Z.M. Li, Efficient electromagnetic interference shielding of lightweight graphene/polystyrene composite, *J. Mater. Chem.* 22 (2012) 18772–18774.

[18] Z. Liu, G. Bai, Y. Huang, Y. Ma, F. Du, F. Li, et al., Reflection and absorption contributions to the electromagnetic interference shielding of single-walled carbon nanotube/polyurethane composites, *Carbon* 45 (2007) 821–827.

[19] M.H. Al-Saleh, U. Sundararaj, Electromagnetic interference shielding mechanisms of CNT/polymer composites, *Carbon* 47 (2009) 1738–1746.

[20] T.K. Gupta, B.P. Singh, V.N. Singh, S. Teotia, A.P. Singh, I. Elizabeth, et al., MnO₂ decorated graphene nanoribbons with superior permittivity and excellent microwave shielding properties, *J. Mater. Chem. A* 2 (2014) 4256–4263.

[21] X. Luo, D.D.L. Chung, Electromagnetic interference shielding reaching 130 dB using flexible graphite, *Carbon* 34 (1996) 1293–1294.

[22] J.G. Park, J. Louis, Q. Cheng, J. Bao, J. Smythman, R. Liang, et al., Electromagnetic interference shielding properties of carbon nanotube buckypaper composites, *Nanotechnology* 20 (1–7) (2009) 415702.

[23] L. Zhang, N.T. Alvarez, M. Zhang, M. Haase, R. Malik, D. Mast, et al., Preparation and characterization of graphene paper for electromagnetic interference shielding, *Carbon* 82 (2015) 353–359.

[24] W.L. Song, L.Z. Fan, M.S. Cao, M.M. Lu, C.Y. Wang, J. Wang, et al., Facile fabrication of ultrathin graphene papers for effective electromagnetic shielding, *J. Mater. Chem. C* 2 (2014) 5057–5064.

[25] B. Wen, X.X. Wang, W.Q. Cao, H.L. Shi, M.M. Lu, G. Wang, et al., Reduced graphene oxides: the thinnest and most lightweight materials with highly efficient microwave attenuation performances of the carbon world, *Nanoscale* 6 (2014) 5754–5761.

[26] W.Q. Cao, X.X. Wang, J. Yuan, W.Z. Wang, M.S. Cao, Temperature dependent microwave absorption of ultrathin graphene composites, *J. Mater. Chem. C* 3 (2015) 10017–10022.

[27] B. Wen, M.S. Cao, M.M. Lu, W.Q. Cao, H.L. Shi, J. Liu, et al., Reduced graphene oxides: light-weight and high-efficiency electromagnetic interference shielding at elevated temperatures, *Adv. Mater.* 26 (2014) 3484–3489.

[28] Y. Xu, K. Sheng, C. Li, G. Shi, Self-assembled graphene hydrogel via a one-step hydrothermal process, *ACS Nano* 4 (2010) 4324–4330.

[29] H.P. Cong, X.C. Ren, P. Wang, S.H. Yu, Macroscopic multifunctional graphene-based hydrogels and aerogels by a metal ion induced self-assembly process, *ACS Nano* 6 (2012) 2693–2703.

[30] H. Sun, Z. Xu, C. Gao, Multifunctional, ultra-flyweight, synergistically assembled carbon aerogels, *Adv. Mater.* 25 (2013) 2554–2560.

[31] J. Lee, J. Kim, T. Hyeon, Recent progress in the synthesis of porous carbon materials, *Adv. Mater.* 18 (2006) 2073–2094.

[32] A.H. Lu, F. Schueth, Nanocasting: a versatile strategy for creating nanostructured porous materials, *Adv. Mater.* 18 (2006) 1793–1805.

[33] T. Morishita, T. Tsumura, M. Toyoda, J. Przeipiński, A.W. Morawski, H. Konno, et al., A review of the control of pore structure in MgO-templated nanoporous carbons, *Carbon* 48 (2010) 2690–2707.

[34] Z.P. Chen, C. Xu, C.Q. Ma, W.C. Ren, H.M. Cheng, Lightweight and flexible graphene foam composites for high-performance electromagnetic interference shielding, *Adv. Mater.* 25 (2013) 1296–1300.

[35] W.L. Song, X.T. Guan, L.Z. Fan, W.Q. Cao, C.Y. Wang, M.S. Cao, Tuning three-dimensional textures with graphene aerogels for ultra-light flexible graphene/texture composites of effective electromagnetic shielding, *Carbon* 93 (2015) 151–160.

[36] Y.Q. Li, Y.A. Samad, K. Polychronopoulou, K. Liao, Lightweight and highly conductive aerogel-like carbon from sugarcane with superior mechanical and EMI shielding properties, *ACS Sustain. Chem. Eng.* 3 (2015) 1419–1427.

[37] M. Inagaki, J. Qiu, Q. Guo, Carbon foam: preparation and application, *Carbon* 87 (2015) 128–152.

[38] H. Hatori, Y. Yamada, M. Shiraishi, Preparation of macroporous carbons from phase-inversion membranes, *J. Appl. Polym. Sci.* 57 (1995) 871–876.

[39] M. Inagaki, N. Ohta, Y. Hishiyama, Aromatic polyimides as carbon precursors, *Carbon* 61 (2013) 1–21.

[40] Y. Hishiyama, S. Yasuda, A. Yoshida, M. Inagaki, Structure and properties of highly crystallized graphite films based on polyimide Kapton, *J. Mater. Sci.* 23 (1988) 3272–3277.

[41] Y. Hishiyama, A. Yoshida, Y. Kaburagi, M. Inagaki, Graphite films prepared from carbonized polyimide films, *Carbon* 30 (1992) 333–337.

[42] Y. Hishiyama, K. Igarashi, I. Kanaoka, H. Fujii, T. Kaneda, T. Koidesawa, et al., Graphitization behavior of Kapton-derived carbon film related to structure, microtexture and transport properties, *Carbon* 35 (1997) 657–668.

[43] M. Inagaki, T. Morishita, A. Kuno, T. Kito, M. Hirano, T. Suwa, et al., Carbon foams prepared from polyimide using urethane foam template, *Carbon* 42 (2004) 497–502.

[44] H. Hatori, Y. Yamada, M. Shiraishi, Preparation of macroporous carbon-films from polyimide by phase inversion method, *Carbon* 30 (1992) 303–304.

[45] H. Hatori, Y. Yamada, M. Shiraishi, H. Nakata, S. Yoshitomi, Carbon molecular sieve films from polyimide, *Carbon* 30 (1992) 305–306.

[46] A.B. Fuertes, D.M. Neveskaia, T.A. Centeno, Carbon composite membranes from Matrimid (R) and Kapton (R) polyimides for gas separation, *Micropor. Mesopor. Mater.* 33 (1999) 115–125.

[47] Y. Li, X.L. Pei, B. Shen, W.T. Zhai, L.H. Zhang, W.G. Zheng, Polyimide/graphene composite foam sheets with ultrahigh thermostability for electromagnetic interference shielding, *RSC Adv.* 5 (2015) 24342–24351.

[48] X.L. Pei, B. Shen, L.H. Zhang, W.T. Zhai, W.G. Zheng, Accelerating the graphitization process of polyimide by addition of graphene, *J. Appl. Polym. Sci.* 132 (1–7) (2015) 41274.

[49] W.S. Hummers, R.E. Offeman, Preparation of graphite oxide, *J. Am. Chem. Soc.* 80 (1958) 1339.

[50] W.T. Zhai, J. Yu, J.S. He, Ultrasonic irradiation enhanced cell nucleation: an effective approach to microcellular foams of both high cell density and expansion ratio, *Polymer* 49 (2008) 2430–2434.

[51] Y. Han, N.K. Mahanta, B. Wang, S. Wang, A.R. Abramson, M. Cakmak, Structural evolution in graphitization of nanofibers and mats from electrospun polyimide-mesophase pitch blends, *Carbon* 71 (2014) 303–318.

[52] M. Pawlyta, J.N. Rouzaud, S. Duber, Raman microspectroscopy characterization of carbon blacks: spectral analysis and structural information, *Carbon* 84 (2015) 479–490.

[53] S. Maiti, N.K. Shrivastava, S. Suin, B.B. Khatua, Polystyrene/MWCNT/graphite nanoplate nanocomposites: efficient electromagnetic interference shielding material through graphite nanoplate-MWCNT-graphite nanoplate networking, *ACS Appl. Mater. Interfaces* 5 (2013) 4712–4724.

[54] M. Murakami, N. Nishiki, K. Nakamura, J. Ehara, H. Okada, T. Kouzaki, et al., High-quality and highly oriented graphite block from polycondensation polymer films, *Carbon* 30 (1992) 255–262.

[55] A. Burger, E. Fitzer, M. Heym, B. Terwiesch, Polyimides as precursors for artificial carbon, *Carbon* 13 (1975) 149–157.

[56] C. Bourgerette, A. Oberlin, M. Inagaki, Structural and textural changes from polyimide Kapton to graphite. I. Optical microscopy and transmission electron-microscopy, *J. Mater. Res.* 7 (1992) 1158–1173.

[57] T. Takeichi, Y. Eguchi, Y. Kaburagi, Y. Hishiyama, M. Inagaki, Carbonization and graphitization of kapton-type polyimide films prepared from polyamide alkyl ester, *Carbon* 36 (1998) 117–122.

[58] J. Su, A.C. Lua, Effects of carbonisation atmosphere on the structural characteristics and transport properties of carbon membranes prepared from Kapton (R) polyimide, *J. Membr. Sci.* 305 (2007) 263–270.

[59] S. Zhao, Z.Q. Shi, C.Y. Wang, M.M. Chen, Structure and surface elemental state analysis of polyimide resin film after carbonization and graphitization, *J. Appl. Polym. Sci.* 108 (2008) 1852–1856.

[60] Y. Isono, A. Yoshida, Y. Hishiyama, Y. Kaburagi, Carbonization and graphitization of shavings filed away from Kapton, *Carbon* 42 (2004) 1799–1805.

[61] D.H. Zhong, H. Sane, K. Kobayashi, Y. Uchiyama, A study of film thickness dependence of the graphitizability of PMDA-ODA polyimide-derived carbon film, *Carbon* 38 (2000) 2161–2165.

[62] H. Konno, K. Shiba, Y. Kaburagi, Y. Hishiyama, M. Inagaki, Carbonization and graphitization having of Kapton-type polyimide film having boron-bearing functional groups, *Carbon* 39 (2001) 1731–1740.

[63] B. Shen, D.D. Lu, W.T. Zhai, W.G. Zheng, Synthesis of graphene by low-temperature exfoliation and reduction of graphite oxide under ambient atmosphere, *J. Mater. Chem. C* 1 (2013) 50–53.

[64] P.A. Thrower, *Chemistry & Physics of Carbon*, CRC Press, 1996.

[65] Y. Hishiyama, M. Inagaki, S. Kinura, S. Yamadas, Graphitization of carbon-fiber/glassy carbon composites, *Carbon* 12 (1974) 249–258.

[66] R.J. Zaldívar, G.S. Rellick, Some observations on stress graphitization in carbon-carbon composites, *Carbon* 29 (1991) 1155–1163.

[67] M. Inagaki, T. Ibusuki, T. Takeichi, Carbonization behavior of polyimide films with various chemical structures, *J. Appl. Polym. Sci.* 44 (1992) 521–525.

[68] W.L. Song, M.S. Cao, L.Z. Fan, M.M. Lu, Y. Li, C.Y. Wang, et al., Highly ordered porous carbon/wax composites for effective electromagnetic attenuation and shielding, *Carbon* 77 (2014) 130–142.

[69] D.X. Yan, H. Pang, B. Li, R. Vajtai, L. Xu, P.G. Ren, et al., Structured reduced graphene oxide/polymer composites for ultra-efficient electromagnetic interference shielding, *Adv. Funct. Mater.* 25 (2015) 559–566.

[70] L. Monnereau, L. Urbanczyk, J.M. Thomassin, T. Pardo, C. Bailly, I. Huynen, et al., Gradient foaming of polycarbonate/carbon nanotube based nanocomposites with supercritical carbon dioxide and their EMI shielding performances, *Polymer* 59 (2015) 117–123.

[71] H.B. Zhang, W.G. Zheng, Q. Yan, Z.G. Jiang, Z.Z. Yu, The effect of surface chemistry of graphene on rheological and electrical properties of polymethylmethacrylate composites, *Carbon* 50 (2012) 5117–5125.

[72] S.T. Hsiao, C.C.M. Ma, H.W. Tien, W.H. Liao, Y.S. Wang, S.M. Li, et al., Using a non-covalent modification to prepare a high electromagnetic interference shielding performance graphene nanosheet/water-borne polyurethane composite, *Carbon* 60 (2013) 57–66.

[73] R. Kumar, S.R. Dhakate, P. Saini, R.B. Mathur, Improved electromagnetic interference shielding effectiveness of light weight carbon foam by ferrocene accumulation, *RSC Adv.* 3 (2013) 4145–4151.

[74] R. Kumar, S.R. Dhakate, T. Gupta, P. Saini, B.P. Singh, R.B. Mathur, Effective improvement of the properties of light weight carbon foam by decoration with multi-wall carbon nanotubes, *J. Mater. Chem. A* 1 (2013) 5727–5735.